This manuscript is the accepted post print of the paper “Modeling of a bidirectional substation in a district heating network: Validation, dynamic analysis, and application to a solar prosumer, Energy, 2023, Vol. 284, art. no. 128621, doi: 10.1016/j.energy.2023.128621”

Modeling of a bidirectional substation in a district heating network: validation, dynamic analysis, and application to a solar prosumer

Giuseppe Edoardo Dino[1,2,*], Pietro Catrini[1], Alessandro Buscemi[1], Antonio Piacentino[1], Valeria Palomba[2], Andrea Frazzica[2]

[1]Department of Engineering, University of Palermo, 90128 Palermo, Italy
[2]CNR ITAE, Salita S. Lucia sopra Contesse 5, 98126, Messina, Italy
[*]Corresponding author’s email: giuseppeedoardo.dino@unipa.it

Abstract

Thermal grids will play a key role in the development of local energy communities and the achievement of 100% renewable societies. Such systems allow excess heat produced by distributed producers through renewable energy sources (also referred to as "thermal prosumers") to be shared among other consumers characterized by high heat demand or who still depend on fossil fuels. However, to achieve more reliable results when performing energy analyses, it is of utmost importance to develop models of prosumers’ substations, where technical details (e.g., type of connections, heat exchangers, valves, etc.) and controllers are accounted for. Starting from the layout of a bidirectional substation for a thermal energy network proposed in the literature, this paper proposes a dynamic model that replicates the experimental setup in the TRNSYS environment. Validation results show a good matching between simulation and experiments in terms of dynamic behavior and energy balance. To show the capabilities of the proposed model, a prosumer with heat available from 205 m^2 solar thermal collectors is considered as a case study. The analysis is performed by assuming two locations characterized by different irradiation values, i.e., Palermo (Italy) and Berlin (Germany). The results show that exchanging the excess heat produced on-site with a heating network allows the solar collectors to reach peak heat production, which is 130 kW and 110 kW for Palermo and Berlin, respectively. The surplus heat sold to the network is equal to 66% and 29% of the total energy exchange within the substation for Palermo and Berlin, respectively. Conversely, the self-consumption of the produced heat accounts for 21.2% and 30.6%, respectively. The model prospectively represents a valuable tool to develop feasibility studies in Thermal Energy Communities and assess the potential of innovative energy- and cost-effective operation strategies.

Keywords

Thermal district, Distributed generation, District heating, Transient simulation, Substations, Solar Energy, Energy Efficiency

1. Introduction

The transition to sustainable models of production and consumption is one of the big challenges in our society [1]. Energy-sharing models could contribute to achieving environmental,

economic, and social sustainability. In this regard, the "Integrated Energy Communities" will offer new opportunities to create smarter, more flexible, and integrated local systems [2]. Although the "Electrical Energy Communities" has already achieved a recognized and organized structure, "Thermal Energy Communities" still need research efforts to overcome some barriers that make their feasibility more difficult [3]. Among those barriers, challenges are related to the capability of dealing with the increasing number of renewable energy producers which could supply heat to thermal grids [4]. Indeed, a typical heat consumer who is connected to the network could become a producer for some hours in a day due to the energy produced by renewable energy plants installed onsite [5]. As in the case of the electricity grid, such an actor is not more classified as "only-consumer", but it is a "prosumer" (i.e., "producer-consumer") [6]. Most of the published papers focused on the benefits achievable by prosumers in District Heating Networks (DHNs) in terms of achievable energy savings and/or the reduction of carbon dioxide (CO_2) emissions. Kauko et al. [7] performed a dynamic analysis of a DHN serving a building area in Norway with the presence of two prosumers (a data center and food retail stores), by using DYnamic MOdeling Laboratory software. The authors found that thanks to the presence of these two prosumers, a 25% reduction in the heat delivered by the central plant could be achieved, with the consequent benefits in terms of "avoided" CO_2 emissions. Gross et al. [8] performed an energy analysis of a low- and ultra-low-temperature DHN with the presence of two prosumers in Germany. The analysis revealed that almost 20% of the total heating demand can be covered by excess heat supplied by the prosumers, and a tool for supporting thermohydraulic analysis of DHN in the presence of prosumers was developed. Other papers focused on DHN thermohydraulic modeling in the presence of distributed prosumers. For instance, Nord et al. [9] showed that the increasing share of heat from the prosumer could lead to a pressure imbalance in the network near the prosumers' substations. However, as observed by the same authors in [9], this problem could be overcome by using variable speed pumps, which could lead, in turn, to electricity savings of 34%. Brand et al. [10] showed that the presence of prosumers could lead to lower supply temperature, local high velocity, and increased fatigue in the pipes. For the case of a 3rd generation DHN operated at 90 °C with a prosumer equipped with solar collectors, the authors estimated that in some cases a 30% reduction in operating temperature could be consequent. Wang et al. [11] performed an energy analysis for estimating the energy benefit achievable thanks to solar thermal prosumers in a Swiss DHN, finding that a solar fraction of 50-63% could be achieved. Huang et al. [12] investigated the potential role of data centers as prosumers in DHN, by considering the coordinated integration of the available heat flows with ones from renewable sources. Li et al. [13] investigated the effects of DHN operating temperatures on the integration

of thermal energy from prosumers. The authors estimated that reducing the operating temperature of DHN from 100 °C to 70 °C could result in cost savings of 2 to 3 percent. Selvakkumaran et al. [14] stressed the urgent need to propose adequate current policies and regulations of DHNs for the integration of prosumers. Postnikov et al. [15] proposed a modeling tool for assessing the reliability of heat supply in DHNs including the presence of prosumers. For one case study, the authors estimated that the amount of heat that would have to be supplied by the prosumer to ensure DHN reliability is not 100 percent of the heat available locally, but nearly 60%. Lickleder et al. [16] developed a thermohydraulic modeling of DHN with prosumers to evaluate the effect of their presence on the DHN. The authors warned about the large sensitivity of the thermohydraulic parameters of the DHN with the increasing number of prosumers.

Most of the previously referenced papers focused on the achievable energy-saving and thermohydraulic effects on DHNs in the presence of prosumers. Regarding substations, very simplified approaches were used in simulations with little attention paid to the controls. Worth noting that substations play a key role in the interaction of producers and/or consumers with the DHN [16]. These systems must exchange heat according to the users' demand profiles or, in the case of onsite production, the thermal energy must be delivered under precise thermal and fluid-dynamic conditions to comply with the standard conditions imposed by the DHN dealer [17]. Although considerable efforts have been made in recent years to improve the design [18] of substations in DHN systems, solve technical issues [19], and monitor the time operation [20], very few works have developed detailed modeling for prosumers' substations [21]. Indeed, when typical consumers decide to become prosumers, the physical layout of existing substations must be modified to allow excess heat produced on-site to be exchanged with the grid while meeting temperature, pressure drop, and flow rate constraints. In this respect, Zinsmeister et al. [22] compared different prosumer system configurations while considering the changes in layout according to the temperature of the DHN and the onsite heat generation system.

There is a need to develop models of prosumers' substations that can be used to better simulate their interaction with the DHN, instead of relying on simplified approaches. The required model should consider technical aspects such as the connections between a user and the grid (e.g., return to supply, supply to supply; etc.), the number and types of heat exchangers used, pumps (variable- or constant- speed), and the embedded control logics to meet temperature setpoint. If these aspects were considered, the reliability of results would increase compared to studies based on highly simplified thermal modeling. In addition, other information can be gleaned from the simulations, which is useful for better understanding the substation's behavior under

different conditions, such as the effects of variable thermal energy production from on-site renewable sources and the temperature at which heat is produced [23]. In the meantime, new control strategies aimed at improving energy savings can be tested [24].

In a recently published paper, Pipicello et al. [25] proposed a layout of a bidirectional substation for a prosumer in DHN along with a detailed experimental characterization of the full- and part-load operation. Considering the literature gap on the modeling of prosumers' substations, this paper proposes a dynamic model that replicates the experimental system proposed in [25], by using the TRNSYS software [26]. The developed model will embed the control logic used to meet the temperature setpoint not only for the water supplied to the served user but also for the temperature of the hot water supplied to the DHN. Based on experimental data available from [25], simulations are first performed to validate the model. Then, to illustrate the capability of the model, an office building is assumed as a potential prosumer thanks to the heat available from solar thermal collectors installed onsite. Note that solar thermal energy was here considered due to the large recognized potential of this source in supplying DHNs [27,28]. Finally, in general terms, the provision of validated modeling of a prosumer substation will then enable:

- the possibility of evaluating the potential heat production of prosumers equipped with different onsite generators (e.g., from renewable cogeneration plants to solar thermal systems [29], from heat pump (HP) [30,31] to low-grade waste heat flows [32]) taking into account temperature and flow rate constraints.
- the possibility of testing new supervisory control strategies aimed at increasing energy savings or solving technical issues (e.g., the high temperature of the return line, pressure drop, and so on).

The structure of the paper is here outlined. In the second section, details on the reference experimental units are provided and the simulation model is presented together with the validation. In the third section, the case study is briefly presented. In the fourth section, the results are presented and discussed. Finally, conclusions are briefly drawn.

2. Materials and Method

In this section, a description of the reference experimental substation is first provided. Then, the modeling and validation are presented.

2.1 Description of the reference experimental substation

Figure 1 shows the layout of the experimental substation developed in [25]. The authors proposed a "*return to supply configuration*" for the substation in [25], according to the layout of substations

presented in [21] and to the outcomes of thermal-hydraulic simulations performed in [33]. In this configuration, the feed-in flow is extracted from the return line of the DHN and heated up to the temperature of the supply line by the local generator (DG). Meantime, the water flow rate returning from the served building is heated up primarily by using the heat produced by the DG, and then, by using hot water drawn from the supply line of the DHN. To manage the bi-directional heat exchange, three heat exchangers are used. More specifically:

- HE1 connects the hydronic loop of the served building directly to the supply and the return lines of the DHN, thus providing thermal energy to the user from the DHN.
- HE2 connects the hydronic loop of the served building to the circuit of the DG.
- HE3 connects the DG directly to the DHN. This heat exchanger is operated to supply the surplus heat produced onsite by the DG to the DHN.

In the experimental set-up presented in [25], the heat produced by the DG is primarily provided to the user through HE2, and in the case of surplus heat, such a flow is delivered to the DHN through HE3. However, such exchange occurs only if the temperature of the water produced by HE3 meets the temperature setpoint of the supply line. If the energy provided by DG is not enough to supply the user load, the DHN will cover the remaining fraction by exchanging heat through HE1. As shown in Figure 1, the testing rig was equipped with a monitoring system composed of temperature, pressure, and flow rate sensors that in this schematic are not indicated, further details can be found in [25].

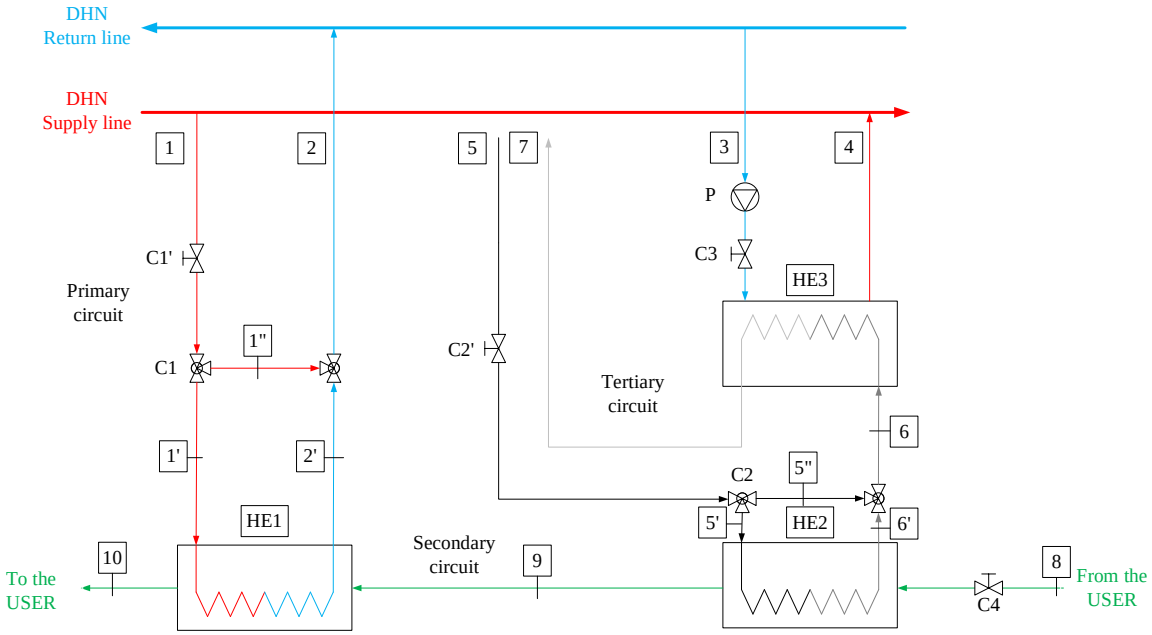

Figure 1. Scheme of the prosumer's substation proposed and tested in [25].

The nominal size of the heat exchangers was selected based on the operating temperatures of the DHN and the hydronic loop of the building. In particular, regarding the DHN, it was considered a return and supply temperatures equal to 50 °C and 80 °C, respectively. These values are typical of a 3rd generation DHN according to [34]. The other nominal temperature levels are 90 °C for the supply line coming from DG, and 60 °C and 40 °C respectively for the supply and return lines of the user circuit. Design parameters are reported in *Table 1*.

Table 1. Design parameters of the heat exchangers of the substation tested in [25].

Heat Exchanger	Primary side		Secondary side	
HE1	F_1,	1.20 m^3/h	F_9	1.80 m^3/h
	T_1,	80 °C	T_9	40 °C
	T_2,	50 °C	T_{10}	60 °C
	Q		42 kW	
	UA		2.90 kW/°C	
HE2	F_5,	3.60 m^3/h	F_8	1.80 0m^3/h
	T_5,	90 °C	T_8	40 °C
	T_6,	80 °C	T_9	60 °C
	Q		42 kW	
	UA		1.20 kW/°C	
HE3	F_3	2.14 m^3/h	F_6	2.80 m^3/h
	T_3	50 °C	T_6	90 °C
	T_4	80 °C	T_7	67 °C
	Q		75 kW	
	UA		5.59 kW/°C	

Check, mixing, and diverting valves were implemented in the testing rig to arrange suitable control management. Referring to Figure 1, it is possible to observe that:

1. C1', C2', and C4 enable or disable the flow passage into respectively primary circuit (HE1), tertiary circuit, and secondary circuit
2. C1 and C2, coupled with their analogous mixing valves attempt to maintain the fluid at the desired set-point temperature

The implemented control logic described in [25] allows coupling the substation with a wide range of DGs and hydronic loops on the user's side (e.g., loop serving fan coils or radiant floor).

2.2 Model description

The described experimental system was reproduced in a virtual environment to create a model that can be scalable and suitable to be implemented into more complex models. The simulation software selected for such a scope was TRNSYS 18. The high flexibility of this software allows for modifying, adding, and connecting several components. In this case, TRNSYS allows for simulating the transient behavior of a substation integrated into a thermal grid in the case of a variable user's demand or a variation of the heating distributed generation (i.e., solar thermal production strictly related to varying weather conditions).

The modeling phase followed two steps. First, the model was replicated in TRNSYS 18, and the resulting layout is shown in Figure 2. Here, each icon, called "type", represents the physical components of the physical system (valves, heat exchangers, and so on) and controllers. Second, its validation was carried out by replicating the dynamic tests performed in [25].

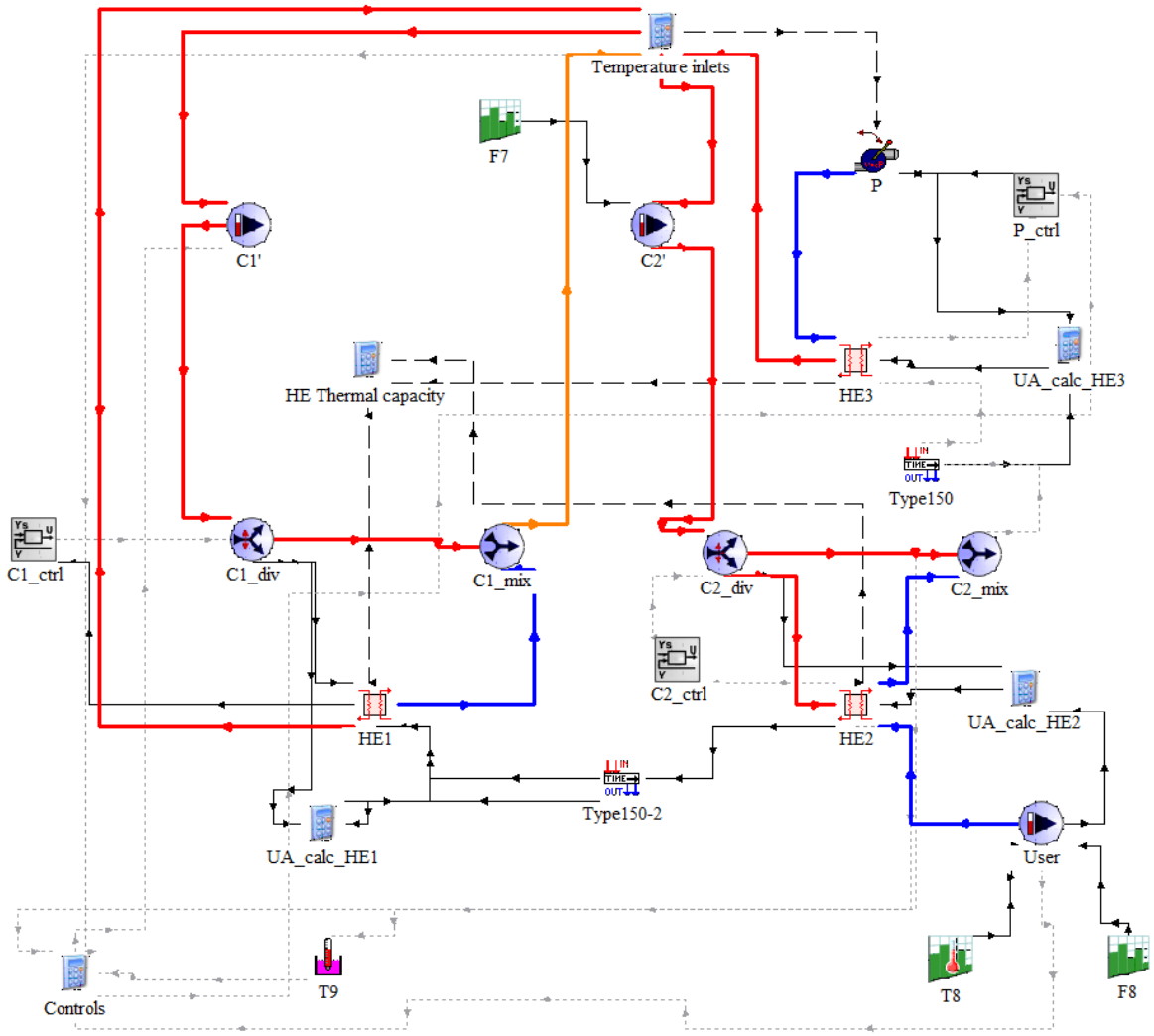

Figure 2. TRNSYS layout of the substation proposed [25].

The heat exchangers were modeled by adopting type 5b (counter-flow heat exchanger). Once the specific heat of fluids flowing in the heat exchanger is set, type 5b requires as input the temperature and flow rate of both fluids and the overall heat transfer coefficient (UA). Since the last one is strictly dependent on the flow rate, a constant value was not suitable for this application. Then, thus, it was necessary to find a factor to correct UA in case of changes in the flow rates compared to the nominal values. In this paper, a very simplified approach was adopted. In particular, knowing the heat transfer coefficient under nominal flow rate conditions UA_n, the aim is to achieve the same coefficient under varied flow rate UA*. The ratio between the heat transfer coefficients is proportional to the Nusselt number ratio that, in this case, can be simply expressed by the Dittus-Boelter expression [35]:

$$Nu = 0.023 Re^{4/5} Pr^{n} \tag{1}$$

Considering that the temperature variation from the nominal conditions is not large (a $|\Delta T| < 30\ ^{\circ}C$ is typically observed for both hot and cold fluids), it was assumed that Pr_n=Pr*, and the ratio between the UA coefficient is proportional to the Reynolds number ratio.

$$Nu = 0.023 Re^{4/5} Pr^{n} \tag{2}$$

$$\frac{UA_n}{UA^*} = \frac{U_n}{U^*} \cong \frac{Nu_n}{Nu^*} \cong \left(\frac{Re_n}{Re^*}\right)^{4/5} \tag{3}$$

Finally, a correlation between flow rate and UA was found as follows:

$$\frac{UA^*}{UA_n} = \frac{\left(\frac{m_h^*}{m_{h,n}}\right)^{4/5} * \left(\frac{m_c^*}{m_{c,n}}\right)^{4/5} * \left[1 + \left(\frac{m_{c,n}}{m_{h,n}}\right)^{4/5}\right]}{\left(\frac{m_c^*}{m_{h,n}}\right)^{4/5} + \left(\frac{m_h^*}{m_{h,n}}\right)^{4/5}} \tag{4}$$

Equation (4) was implemented in a calculator type that, for given nominal and operation flow rates on the hot and cold sides, calculates the overall heat transfer coefficient for each heat exchanger and each simulation time step. This approach gives high flexibility to the model that can be scalable for several applications.

As previously mentioned, the valves C1' and C2' in Figure 1 enable the flow passage, according to the control logic here used; they were replaced with pumps (type 110) in the model and they were operated by maintaining the same algorithm used in the experimental set-up to control the valves. The diverter and mixing valves were modeled by type 11f and type 11h, and the flow rate splitting on the diverter is controlled by an iterative feedback controller (type 22). This controller

was implemented to model a real feedback controller (e.g. PID) that would adapt its control signal continuously or use a discrete timestep much shorter than the TRNSYS simulation timestep. The "C1_ctrl" represented in *Figure 2* reads the controlled variable T_{10} and sends a signal to the diverter valve C1 that changes the flow rate coming to the primary side of HE1 from the supply line of DHN to maintain the controlled variable T_{10} at the fixed set point (60 °C). Analogously, "C2_ctrl" acts on the diverter C2 to maintain T_9, as far as possible, at 60 °C by varying the water flow coming from the DG and entering the primary side of HE2.

Since the first simulations revealed instability due to the mutual interaction between the controllers, a delay effect (type 150) was introduced to solve this issue. Worth noting that such a delay well represents the hydraulic inertia of the system.

Finally, the pump "P" indicated in the experimental layout (Figure 1) was modeled by using type 741. An iterative feedback controller sends a signal to variate the flow rate in the pump, by assuming the outlet temperature on the load side of the HE3, T_4, as the controlled variable. In particular, the controller aims at maintaining T_4 at 80 °C. The pump is stopped when, on the source side of HE3, the inlet temperature T_6 is lower than a minimum value, here fixed at 82 °C. This function ensures a stable feed-in temperature on the DHN supply line.

The pump controls were implemented in the calculator type "Controls" and they replicated the ones adopted in the experimental rig. Details on such control logic are provided in Appendix A.

2.3 Model validation

In the experimental study, three dynamic tests were performed by varying temperature and flow rate on the three circuits, to replicate the system operation under severe conditions. The operating conditions of these tests as reported in *Table 2*. The variation in the user demand was simulated by varying the user return temperature (T_8) and the flow rate (F_8), and a variable DG profile was achieved through a predefined flow rate variation profile (F_7).

Table 2. Operating conditions of the experimental tests performed in [25].

	Test_prod_only	Test_cons_only	Test_pros
HE1	Not operating	Operating	Operating
HE2	Operating	Operating	Operating
HE3	Operating	Not Operating	Operating
F_2 [m^3/h]	-	1.80	1.80
F_7 [m^3/h]	2.80	2.80	0.90-2.80
F_8 [m^3/h]	0-1.80	1.80	0-1.80
T_1 [°C]	-	80	80
T_3 [°C]	50	-	50

T_4 [°C]	80	-	80
T_5 [°C]	90	90	90
T_8 [°C]	40-50	30-40	40-50
T_{10} [°C]	60	60	60

Figure 3 graphically depicts the operation of the three heat exchangers in the proposed tests. Test_prod_only was focused on the operation of HE2 and HE3 under different levels of user thermal demands (Figure 3a) and it is based on the DG production that is partly destinated to the self-consumption and partly to the DHN; Test_cons_only, analogously to the previous one, tested the performances of the substation when HE1 and HE2 are operated (Figure 3b) and is based to the "consumer" mode in which the DG and DHN satisfy the entire demand; finally, Test_pros combined the boundary conditions imposed for the previous tests and evaluated the system by operating all the heat exchanger by varying the user load and the DG energy production profile (Figure 3c) and represents the full "prosumer" condition.

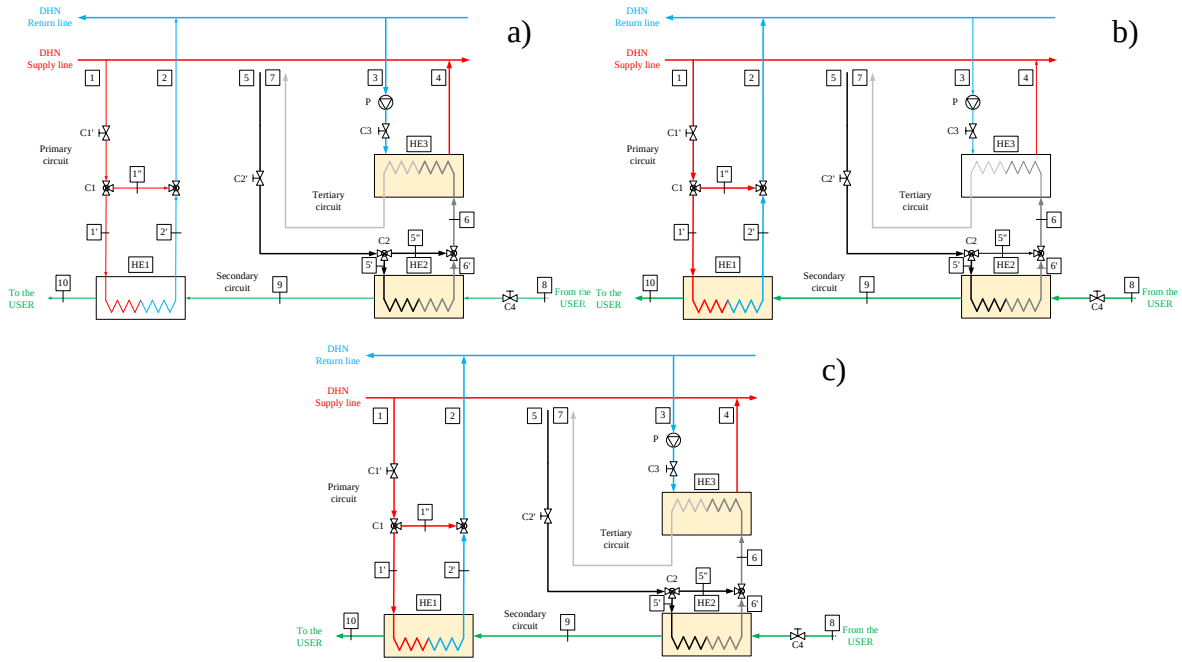

Figure 3: Focus on heat exchangers and lines activated for each test. a) Test_prod_only, b) Test_cons_only, c) Test_pros

The tests reported in Table 2 were replicated in the model through schedule TRNSYS types implemented in type 14h and type 14e and a comparison between experimental and simulation results was carried out. The simulation time step was fixed at 1 minute to better represent the operation of the iterative feedback controller. The simulated time was equal to the one used in the experimental campaign (i.e., seven hours). The test conditions imposed for each test are shown in Figure 4. The simulation results were compared with the experimental results presented in [25].

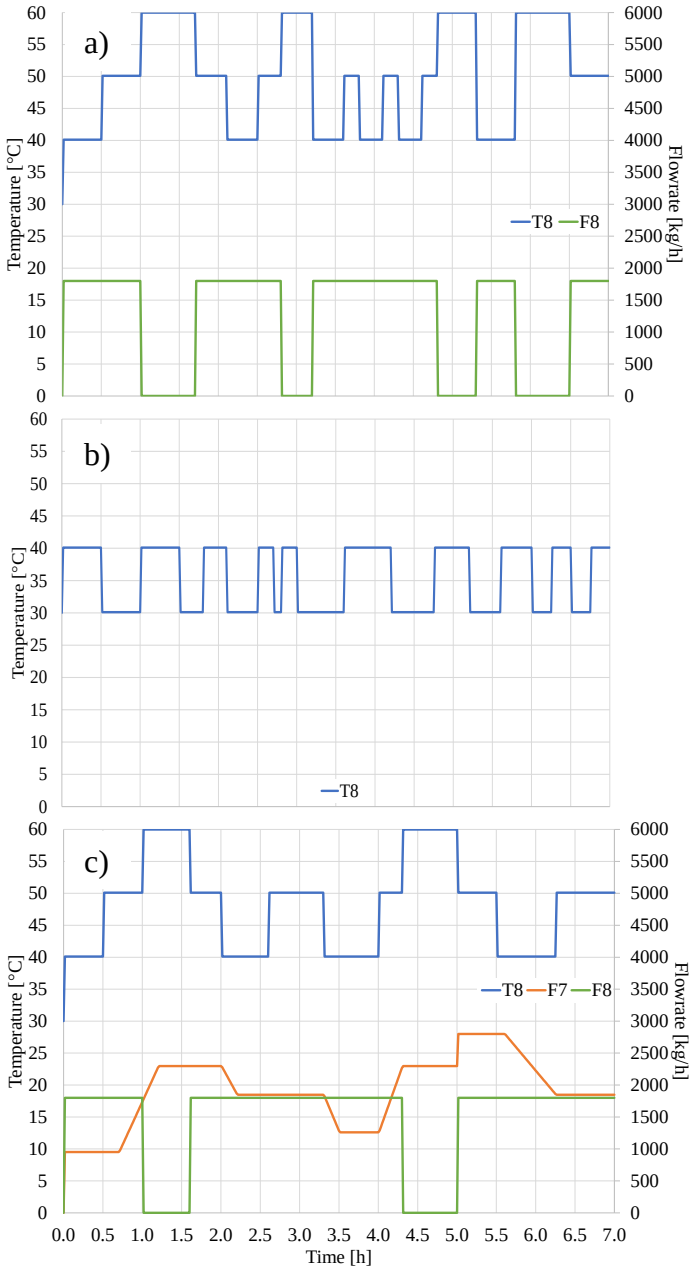

Figure 4. Dynamic conditions imposed on the experimental tests carried out in [25] and replicated in the virtual model. a) Test_prod_only - b) Test_cons_only - c) Test_pros.

In Test_prod_only, the flow rate and temperature of the user return line were varied according to a defined schedule shown in Figure 4a. More specifically, T_8 was varied between 40 °C and 50 °C (maximum and minimum load for Test_prod_only), and the flow rate was switched between 1800 kg/h (nominal value) and 0 kg/h (no user demand). The simulation results show a good match with the experimental ones. In this respect, the temperature profile at the outlet of HE1 (T_{10}), HE3 (T_4), and C2 mixer (T_6) are shown in Figure 5.a. The profiles for heat transfer shown in Figure 5.b showed a good match for HE2, whereas for HE3, a slight difference was found. However, since

the difference between simulated and experimental values was always lower than 10% for Test_prod_only, the model validation was considered satisfactory.

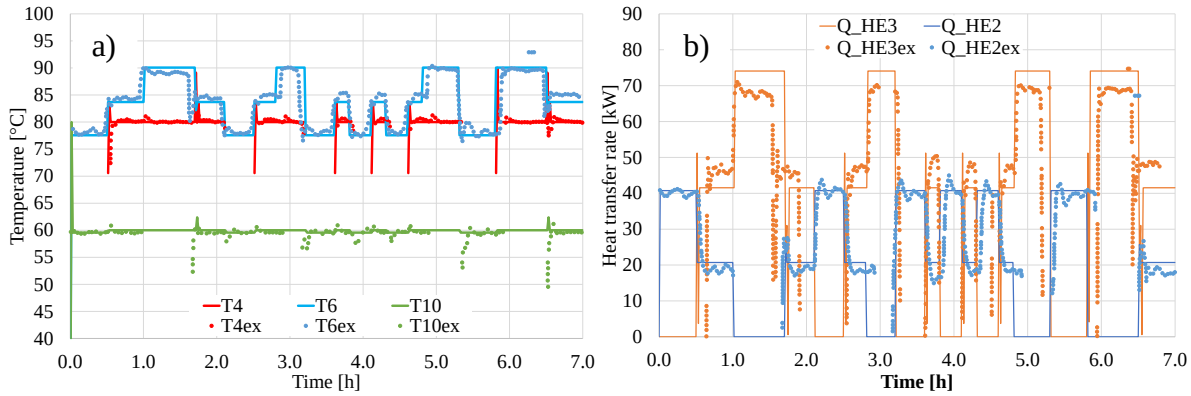

Figure 5. Comparison between simulated and experimental results for Test_prod_only: a) temperature profiles - b) heat exchanged on HE2 and HE3.

In Test_cons_only, only T_8 was varied with a defined schedule between 30 °C and 40 °C (maximum and minimum load for the test), and the maximum demand from the users required the operation of both HE1 and HE2. As in the previous test, a good matching was achieved for temperature and heat transfer rate profiles, with a better correspondence for HE1 rather than HE2. However, a difference lower than 5% between experimental and simulated values was found (Figure 6).

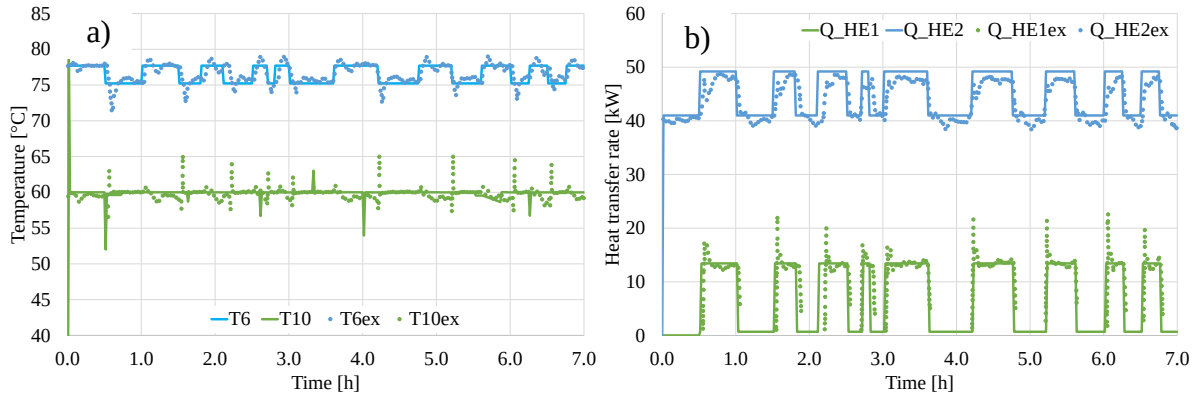

Figure 6. Comparison between simulated and experimental results for Test_cons_only. a) temperature profiles - b) heat exchange on HE1 and HE2

Test_pros combines variable profiles of the user's demand and DG production, thus involving the operation of all heat exchangers. As shown in Figure 7.a-b, the simulated temperature and heat transfer profiles are like the experimental ones. In both figures, the experimental profiles for T_4 and the heat transfer rate of HE3 show an oscillating behavior between 4-6 hours and 6-7 hours that is not replicated by the simulation results. This is due to the typical thermostat on/off behavior

that was not replicated by the simulation model. Conversely, the model reflects both stationary and dynamic trends when no frequent on/off operations occur.

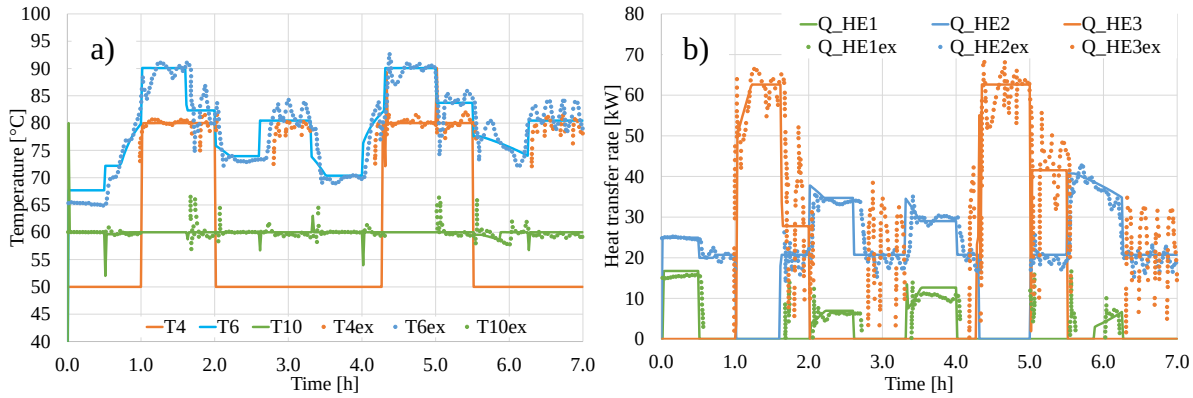

Figure 7. Comparison between simulated and experimental results for Test_pros: a) temperature profiles - b) heat exchanged in HE1, HE2, and HE3.

3. Case study

Among renewable energy sources for heat supply in DHNs, solar thermal energy is recognized to play a key role in the decarbonization process [36,37]. In this regard, in Europe, several DHNs supplied by solar thermal technologies are successfully operating with some promising results [27,38]. For this reason, the effect of coupling a bi-directional thermal substation with a solar heating system was here investigated. More specifically, the solar thermal system was composed of high vacuum solar collectors whose data, retrieved from the Solar Keymark certificate, are reported in Table 3 [39]. The performances of the chosen high vacuum solar thermal collectors are aligned to those presented in (reference), coherently with solar Keymark data.

Table 3. Solar Keymark Parameter of the chosen high vacuum solar thermal panel.

Parameter	Value	Unit
Zero loss efficiency (η_0)	0.732	-
First-order coefficient (a_1)	0.50	W/m^2K
Second-order coefficient (a_2)	0.006	W/m^2K^2
Incidence angle modifier IAM (50°)	0.95	-

An office building characterized by a peak of 100 kW_{th} in thermal demand was assumed as the reference user. Two different climates were chosen to evaluate the behavior of this prosumer: Palermo (Southern Italy, Csa climate according to Köppen classification) and Berlin (Germany, Cfb climate according to Köppen classification). Both weather files were retrieved from

METEONORM [40] database ("Palermo Punta Raisi" and "Potsdam"). The yearly load profiles of the heating demand for the selected sites are shown in Figure 8-a.b. It is worth noticing that these profiles were developed by using a "synthetic load" approach, whose details are provided in Appendix B. The simulation was performed for one year of operation.

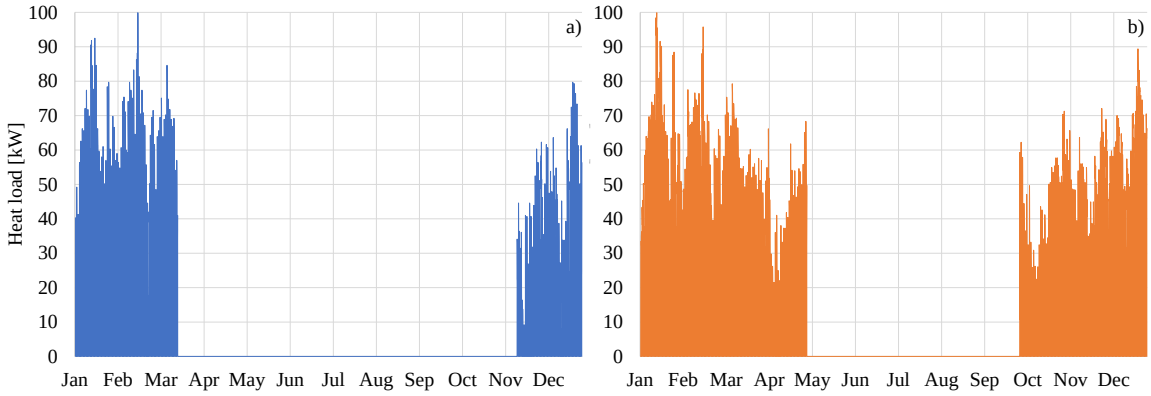

Figure 8. Heat load profile for the selected sites: Palermo (a) and Berlin (b).

The monthly energy request is shown in Figure 9. Yearly, the total amount of heat requested is 78,923 kWh/y in the case of Palermo and 151,051 kWh/y for Berlin.

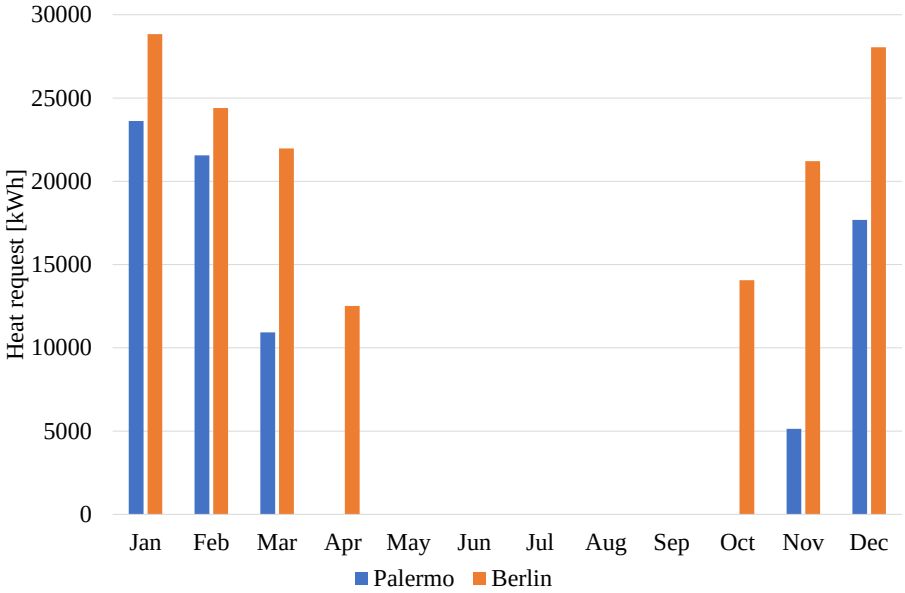

Figure 9. Monthly heating energy demand in the selected sites.

The design of the solar DG system was performed according to the peak value of the thermal demand of the user and the nominal operating temperature of the DHN lines. These temperatures were assumed to be equal to 50 °C for the return line and 80 °C for the supply line. A net solar collector surface of 205 m^2 was considered with a temperature outlet set point of 95 °C, a slope of 30°, and a south-facing azimuth angle. The TRNSYS type 539 was selected to model the solar

field. This type tries to keep the collector outlet to the outlet set-point temperature by varying the water flow rate. In addition, it shuts off the collector (flowrate = 0) if the collector is losing energy. This condition occurs when the control system detects a negative temperature difference at the outlet and inlet of the collector. Finally, it accounts for the effect of the collector heat capacity. A safety controller was implemented to dissipate the solar heat surplus through a dry cooler (type 511), thus avoiding overheating and stagnation of solar panels. Finally, the solar field was connected to a stratified buffer tank (type 340) with a nominal volume of 20 m^3 that allows for equalizing the daily peak energy production of the solar system and the distributed energy request by the user. The layout of the solar loop is shown in Figure 10.

The overall control logic of the substation was not changed compared to the one proposed in [25]. In particular, the control logic tries to maximize the exploitation of the heat produced by the solar collectors through HE2 and HE3, and it operated HE1 as a backup to cover the fraction of the thermal demand not met by heat available from solar collectors.

The simulation time step was fixed at 1 hour according to the variation of climatic variables and user demand. Finally, the efficiency of solar collector $\eta_{\mathrm{sol}}^{\mathrm{gross}}$ was calculated as indicated in Eq. 5:

$$\eta_{\mathrm{sol}}^{\mathrm{gross}} = \int \frac{\dot{Q}_{\mathrm{sol}} dt}{G_{\mathrm{col}} * A_{\mathrm{sol}}^{\mathrm{gross}}} dt \tag{5}$$

where: $\dot{Q}_{\mathrm{sol}}$is the instantaneous thermal power output expressed in kW, $G_{\mathrm{col}}$is the specific solar irradiation on the collector plane measured in kW/m^2, and *A* is the solar collector's gross surface area (measured in m^2).

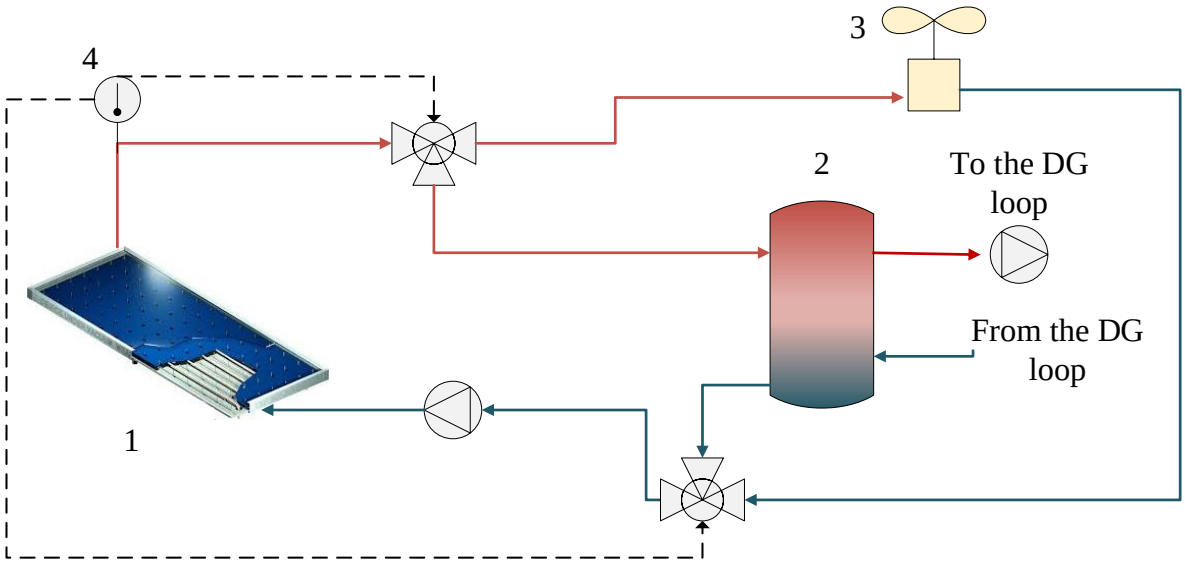

Figure 10: Layout of the solar loop. 1) High vacuum solar collectors, 2) Storage tank, 3) safety dry-cooler, 4) safety thermostat controller

4. Results and Discussion

The results of the performed dynamic simulations are presented and discussed in the following subsections for a typical week in winter and summer. Some insights on substation operation are also given to allow for a keener interpretation of the interactions among components and controls. Then, yearly energy results are presented. Finally, a discussion on the main findings, limitations, and future development of this work is made.

4.1 Results obtained for a typical week in winter and summer

Figure 11.a-b depicts the profiles of the heat transfer rate for each heat exchanger together with the user heating demand, for six typical winter days (more specifically from January 25th to January 31st) in Palermo (Figure 11.a) and Berlin (Figure 11.b). Note that:

- in the case of Palermo (Figure 11.a), HE2, which is supplied by the hourly thermal energy produced by the solar DG, can meet a large fraction of the user heat demand (between 25% and 100%, as indicated by the blue line), except for the last day in which the relative weight of HE1 is predominant due to the low amount of heat provided by the solar DG.
- in the case of Berlin (Figure 11.b), a lower amount of heat is provided by the solar field through HE2, and the heating demand is mostly covered by HE1.

The heat transfer rate for HE2 is equal to 30 kW for Palermo and 22 kW for Berlin. In both cases, since the energy produced by the DG is entirely exchanged in HE2, the HE3 is always off. Note that HE3 does not operate for most of the heating period.

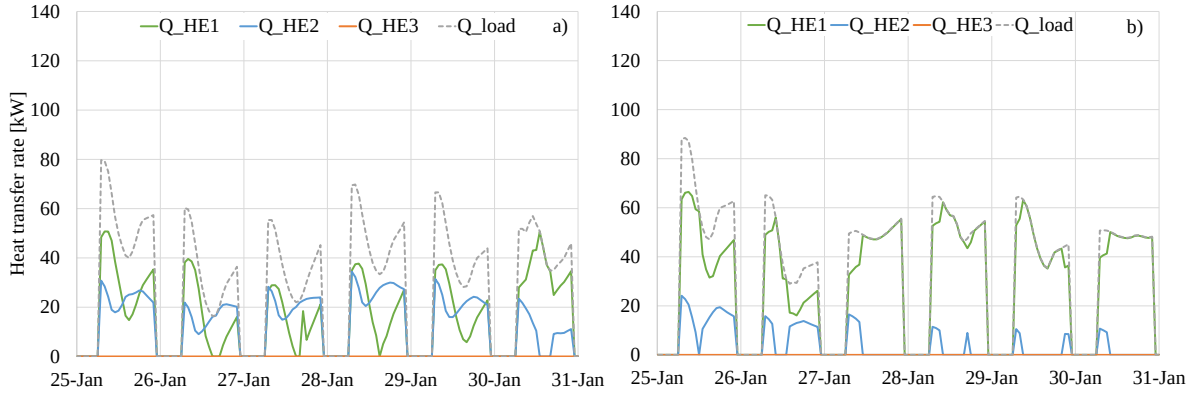

Figure 11. Heat exchangers dynamic trend for six typical winter days: a) Palermo - b) Berlin.

In Figure 12.a-b the temperature profiles on the user loop (indicated in Figure 1 as T8, T9, T10,) are shown along with the inlet temperatures on the hot sides of HE1 and HE2 (T1, T5) for a winter day (more specifically, for January 25th, corresponding to the first day of the selected winter period). Following the substation layout shown in Figure 1, the water flow coming back from the hydronic circuit of the building (with a temperature equal to T8) is first heated up by the DG loop through HE2 (T5, inlet on the hot side), then by HE1 (T9 inlet on the cold side). HE1 is activated since the required set-point for T10 is not met. Worth noting that in the case of Palermo (Figure 12.a), T5 values are higher than the one observed in Berlin (Figure 12b), with an average difference of 5 °C. The user flow F8 leaves HE2 by maintaining an average temperature difference with T8 of 6 °C for Palermo and 5 °C for Berlin. In both cases, T10 is equal to the desired set-point (60 °C), thus suggesting that the controller C1_ctrl1 is properly controlling the amount of water flowing through HE1. Finally, the temperature of the water exiting HE2 (T9) is higher in the case of Palermo, thus justifying the lower energy contribution of HE1 in this site.

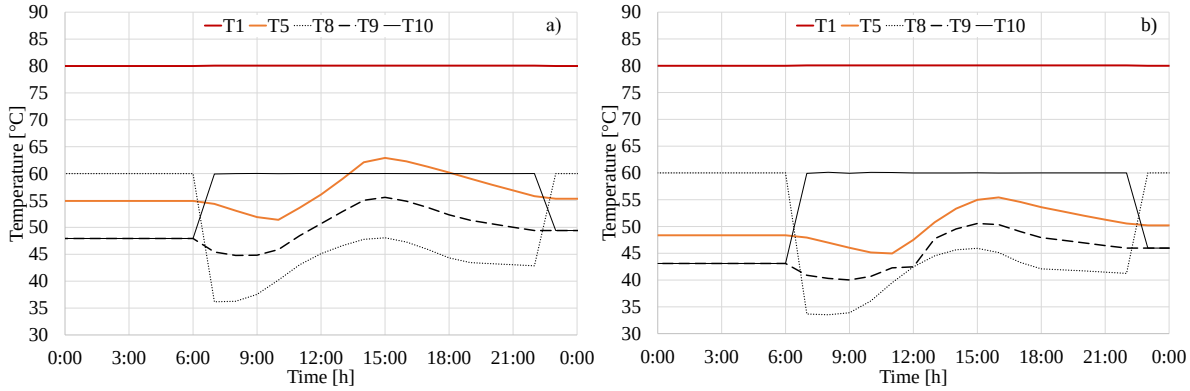

Figure 12. Temperature trends for the user temperatures loop and inlet temperatures on the hot side of HE1 and HE2 for a typical winter day (January 25th): a) Palermo - b) Berlin sites.

Figure 13.a-b shows the profiles of the heat exchanged in all heat exchangers for six typical operation days in summer in Palermo (Figure 13.a) and Berlin (Figure 13.b). In this case, there is

no heating demand from the user, so HE1 and HE2 are always off. In the case of Palermo (Figure 13.a), the thermal power exchanged with DHN through HE3 is equal to 130 kW, and the heat exchanger is operated for almost 6.5 hours per day. This is due to the continuous availability of hot water at a temperature that is higher than the desired set-point (85 °C) on the inlet of the heat exchanger's hot side (T6). In Berlin (Figure 13.b), although the peak heat transfer rate ranges between 100-110kW, the profile shows an oscillating behavior due to the lower amount of energy produced by DG and the unavailability of hot water at the desired set-point. Once activated the HE3, the buffer tank is rapidly discharged by the energy stored and the controllers stop the operation of the pumps that provide the flow rate on the DG loop (hot side) and DHN loop (cold side).

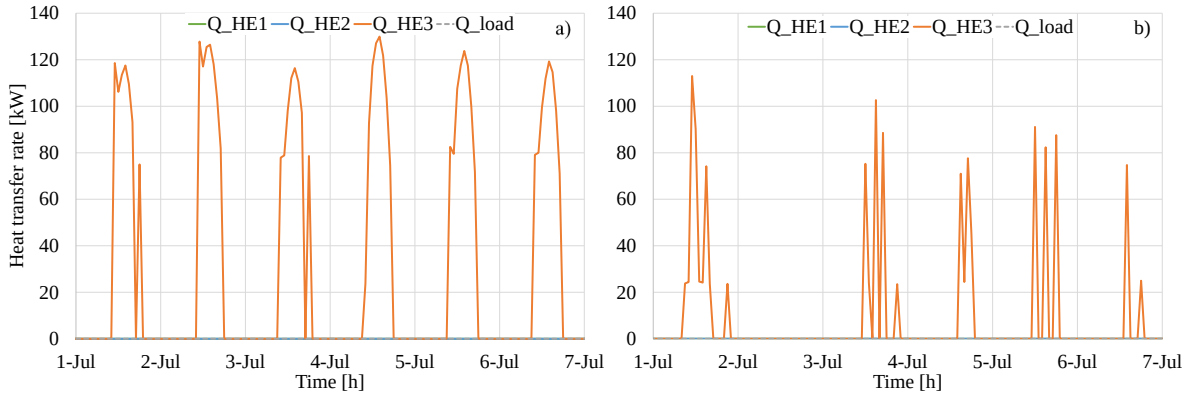

Figure 13. Heat exchangers dynamic trend for six summer operation days. a) Palermo - b) Berlin.

In Figure 14.a-b the temperature profiles on HE3 are shown for a typical summer day in which there is no heat request from the user and thus HE1 and HE2 are not operating. Following the substation layout shown in Figure 1, the hot water flows from the storage tank to C2' is delivered directly to HE3, and finally, it flows back into the storage. On the cold side of the heat exchanger, the pump "P" is activated when the set-up conditions are respected (please, refer to sections 2.1, 2.3 and Appendix A) and modulates the flow rate to achieve the desired outlet temperature (DHN supply temperature). In both cases, the flow leaves the heat exchanger at the same temperature (T7=T4) when the pump is activated. It is worth noticing that in Palermo the average inlet temperature on the hot side (T6) is higher than the one observed in Berlin due to higher irradiation values. In Figure 14 is possible to notice the on-off operation due to the satisfaction of the inlet temperature requirement on the hot side of HE3 (T6). When T6<85 °C HE3 is not activated.

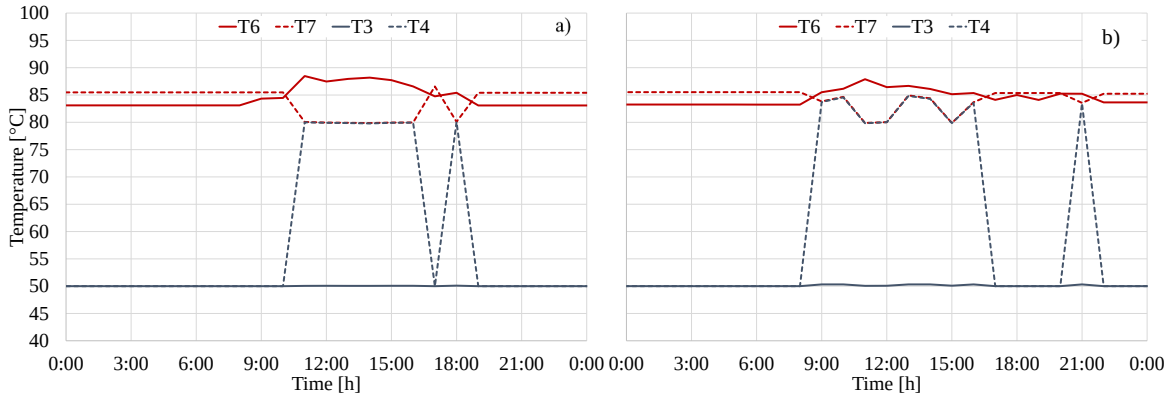

Figure 14: Temperature trends for HE3 for a typical summer day (July 1st): a) Palermo - b) Berlin sites

4.2 Results for the solar field

The energy production of the solar field in the selected winter week ranges between 40 kW and 90 kW for Palermo and between 38 kW and 73 kW for Berlin (respectively Figure 15a and Figure 15b). Solar radiation is related to the total net tilted surface of collectors. In Palermo, the outlet temperature set point (95 °C) is achieved for each day of the selected period and maintained constant for almost all the diurnal hours except for the last day due to the low solar radiation.

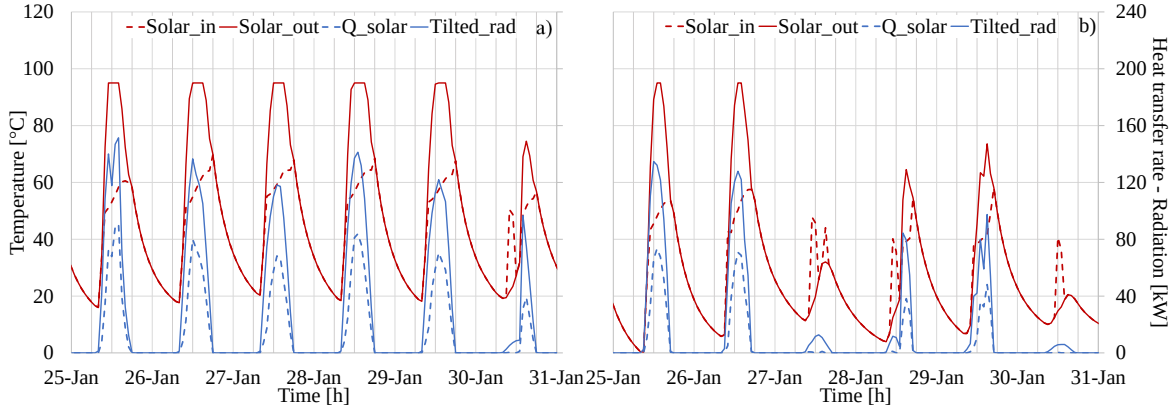

Figure 15. Profile of solar energy production and temperature profiles on a typical winter week: a) Palermo - b) Berlin.

The energy produced by the solar DG in the selected summer week ranges between 120 kW and 135 kW for Palermo and between 11 kW and 104 kW for Berlin (Figure 16a and Figure 16b). Since there is no heat demand from the user, all the energy produced by the collectors is delivered to HE3. Furthermore, the solar energy surplus which is not rejected through the dry cooler is delivered to the DHN when there is no heating request by the user. By using the proposed substation, energy savings is twofold: on one hand, the dry cooler is never activated, thus avoiding energy consumption for running the fans. On the other hand, the energy exchanged with DHN,

produced by solar collectors, allows for a reduction of the energy produced by those centralized plants that supply the DHN, which typically use natural gas or biomass as primary fuels.

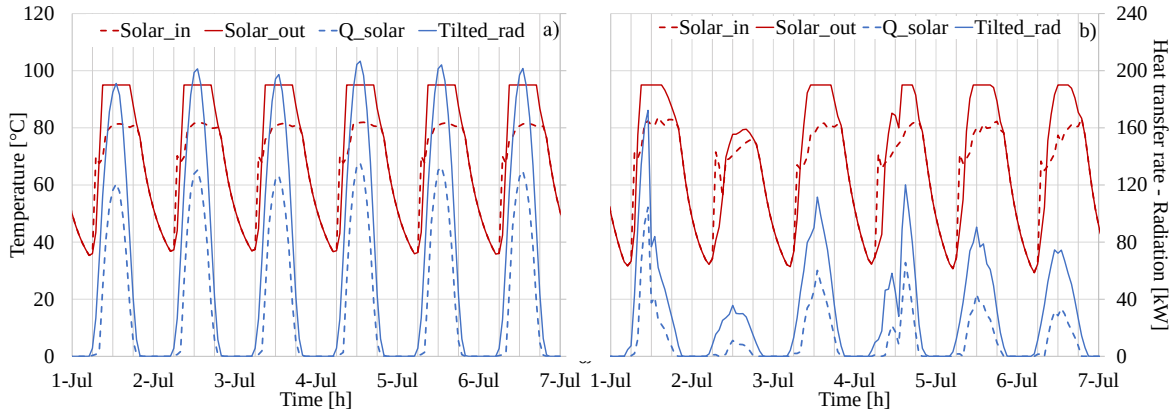

Figure 16. Profiles of solar energy production and temperature for the typical week in summer: a) Palermo - b) Berlin.

The total solar energy produced in the simulated period is 217.6 MWh for Palermo and 114.1 MWh for Berlin. Then, by using Eq. 4, the following efficiencies were found: $\eta_{\mathrm{sol}}^{\mathrm{gross}} = 0.52$ in the case of Palermo and $\eta_{\mathrm{sol}}^{\mathrm{gross}} = 0.45$ in Berlin.

4.3 Yearly energy results

Starting from the case of Palermo, Figure 17.a shows the total energy balance of the substation. More specifically, it displays the ratio between the energy transferred by each HE and the total energy exchanged within the substation. As shown in Figure 17.a, the heat produced by the solar system and transferred to the DHN (via HE3) represents the maximum contribution to the overall energy exchanged, accounting for almost 66%. The heat produced by the DG and supplied to the user (via HE2) accounted for 17.7%. The heat supplied by the DHN to the user (via HE1) accounted for 16.3%. Figure 17.b show the fractions of the heat produced by the solar system, which are supplied to the user and delivered to the DHN. It is worth noting that the main contribution belongs to DHN (79% for HE3), which is due to the correspondence between the period of high radiation (summer) and the absence of heat demand from the user. This information is useful for optimizing the design of the solar system.

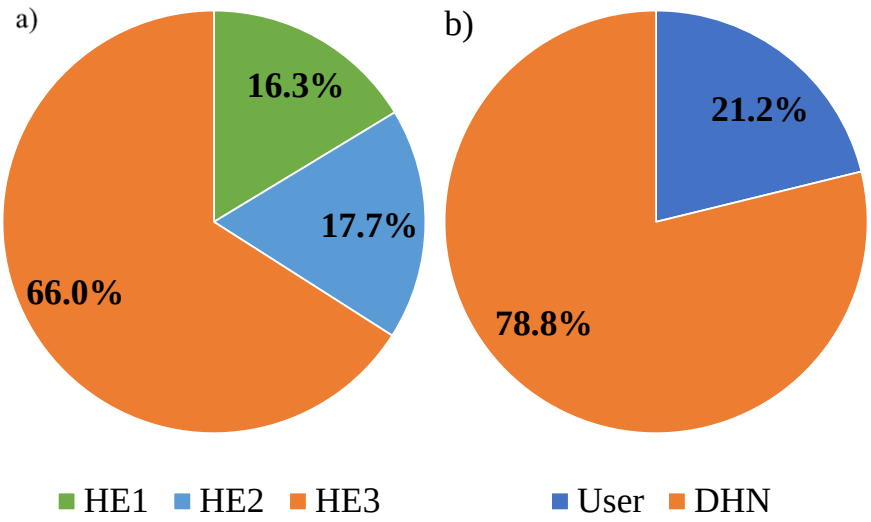

Figure 17. Energy balance on the heat exchangers (a) and DG energy distribution between the user and DHN in the case of Palermo.

Similarly, Figure 18.a-b shows the total energy balance of the substation and DG in the case of Berlin. Looking at Figure 18.a, it is worth noting that the heat drawn from the DHN represents the maximum contribution to the substation balance (accounting for 56.9%). In addition, a relevant role is also played by HE3 in which 29.9% of the total amount of the exchanged heat by the substation is transferred to the DHN, while only 13.2% of the thermal energy exchanged is delivered to the user due to the low radiation during the winter period. As regards the energy balance of the DG, as shown in Figure 18.b, a large fraction of the heat produced is supplied to the DHN (69% for HE3).

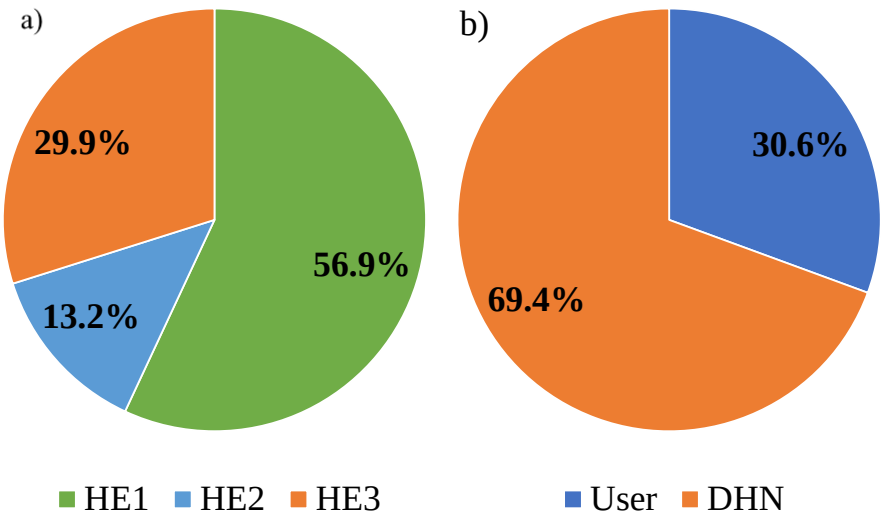

Figure 18. Energy balance on the heat exchangers (a) and DG energy distribution between user and DHN in the case of Berlin.

4.4 Findings, limitations, and future developments of the present work

The above analysis highlights the importance of including detailed thermal modeling of a prosumer's substation for a more accurate estimation of the amount of energy exchanged between the prosumer and the grid. First, as shown in Figure 12 and Figure 14, the possibility to monitor temperature values in the substation allows for checking the meeting of the set point for the hot water supplied to the buildings and the water supplied to the DHN. In this regard, even if heat could be available from the DG, the produced heat flow is supplied to the grid only if the temperature setpoint of the produced hot water is properly met. This capability avoids the risk of overestimating the potential energy savings arising due to the presence of prosumers, which could occur when relying on a very simplified substation layout [13] or when using an energy approach [15]. In addition, the inclusion of feedback controllers allowed for (i) a more realistic description of controller actions (typically, performed by using inequality constraints [16]), and (ii) a better description of the coordinated operation between the substation and the DG. Indeed, as shown in Figure 13.b, the temperature set-point on the thermal storage leads to a discontinuous supply of heat to the DHN. Finally, the annual results show that solar collectors are a promising technology for prosumers in DHNs, although large differences in thermal energy sharing (e.g., self-consumption or heat selling) exist according to the assumed locality (see Figures 17 and 18). The possibility to accurately describe such sharing is then useful for the development of a refined control strategy that aims at optimizing the economic results achieved by the prosumer.

As the main limitation of the virtual modeling proposed in this study, it can be noted that it is suitable for accurately performing only the thermal analysis of the prosumer’s operation, as

hydraulic modeling is not considered. In this regard, future research will aim to also include these aspects to describe pumps' operation and quantify the electrical energy consumed. In addition, the lack of constraints arising from the existence of heat demand from the DHN can be considered a further limitation of the proposed study. Indeed, if the deficit in heat production can be replaced by using the DHN, the surplus heat produced by the local DG can be critical when the architecture of the DHN is not known or not defined. A detailed heat dispatching model is then needed to better understand if a DHN can receive the huge amount of heat available from intermittent renewable energy sources. In future research, it is of utmost importance to include a supervisory control architecture that allows the exchange of information between the prosumer and the DHN dealer regarding the actual need of the DHN for the heat produced onsite by the DG. In addition, the flexibility given by the control logic will allow proposing new algorithms arising from "third party access" contracts [41,42]. Future works will enhance the proposed prosumer substation structure, by including heat price and third-party access options on a more complex and articulated system.

5. Conclusions

In this paper, thermal modeling of a prosumer's substation in DHNs was presented, which was implemented in TRNSYS 18 environment and validated against experimental results available in the literature for a similar setup. Results showed a good agreement between experimental and simulated results for both the energy and thermal response of the system, with relative errors lower than 5% or 10%, respectively. Assuming a 205 m^2 solar thermal field composed of high vacuum solar thermal panels as a district generation plant, simulations were performed for two different geographical locations, i.e. Palermo (Csa-Köppen classification) and Berlin (Cfb-Köppen classification). Based on the local solar irradiance levels, the solar collectors achieved heat capacity peaks in the order of 130 kW for Palermo and 110 kW for Berlin. Results showed that the prosumer substation allowed for a total exploitation of the heat produced by the solar distributed generation system, thus avoiding any waste of excess heat production from the solar source into the environment; also, the embedded controls could provenly meet the desired water temperature setpoints. In the presence of an unstable energy source, such as the solar one, the examined substation with bi-directional heat exchange allows for full energy exploitation to supply the final user, through the heat purchase from the DHN in case of a lack, or sale to the network in the case of an excess of local production by the solar DG. In the examined configuration, the surplus heat supplied to the grid ranged between 29% and 66% of the total amount of energy exchanged by the substation, while the self-consumption accounted for up to 21.2% and 30.6%, respectively for Palermo and Berlin. Being the solar source not sufficient to supply the heat

demand, the need for a relevant heat supply from the DHN was assessed, accounting for 16.3% and 56.9% of the total exchanged heat for Palermo and Berlin, respectively.

These results highlight the crucial role that a substation with bi-directional heat exchange can play to promote distributed heat generation by intermittent renewables such as solar energy. In DHNs comprising large users with continuous or asynchronous heat demands (large tertiary, sports centers, hospitals, etc.), the surplus heat produced by solar plants and supplied to the network could be effectively exploited by these remote users, lowering the share of heat produced by fossil fuels or electricity in conventional boilers or heat pumps. The proposed model represents a viable tool to perform analyses aimed at identifying the optimal capacity and spatial distribution of such distributed renewable systems, for a given set of prosumers connected to the network, and to investigate rational pricing mechanisms to promote effective coordinated management of equipment. In the next future, further research will be aimed at refining the model with additional hydraulic analysis and evaluating the influence of the dynamic behavior of energy users within the integrated energy communities.

Acknowledgments

This study was developed in the framework of the research activities carried out within the PRIN 2020 project: "OPTIMISM—Optimal refurbishment design and management of small energy micro-grids", funded by the Italian Ministry of University and Research (MUR).

Appendix A

The pump activation controls that replicate the ones set in the experimental rig were implemented in the calculator type "Controls". In this calculator a set of equations was introduced to model the operating conditions that let to allow the flow rate circulation in the primary circuit by activating valve C1', in the tertiary circuit by activating valve C2', and in the cold side of HE3 by activating the pump P (Figure 1). The control equations are detailed below:

- C1' is activated if $\begin{cases} T_9 < T_{9,\text{SETPOINT}} \\ F_8 = 0 \end{cases}$ $T_{9,\text{SETPOINT}}$ is monitored by a thermostat that is set at 59 °C with a centered dead band of 1 K
- C2' is activated if $\begin{cases} T_5 < T_8 + \Delta T \\ F_8 = 0 \end{cases}$ V $\begin{cases} T_6 > T_{\text{min,DHN}} \\ F_8 = 0 \end{cases}$ ΔT=5K, $T_{\text{min,DHN}}$=82 °C
- P is activated if $\begin{cases} T_6 > T_{\text{min,DHN}} + \Delta T \\ F_7 > 0 \end{cases}$ $T_{\text{min,DHN}}$=82 °C

Appendix B

The Building Energy Signature (BES) [43] and [44] can be used to quickly characterize the hourly distribution of the thermal loads of a building whenever the influence of both internal and solar heat gains is neglected. As first introduced by [45] and described in the EN 15603 standard [46], BES is defined as the thermal power P_b required by a building as a function of the dry bulb temperature of the outdoor air T_{ext}.

$$P_b(i) = P_{des} \cdot \left[\frac{T_{HLET} - T_{ext}(i)}{T_{HLET} - T_{des}} \right] \quad \text{(A.1)}$$

In Eq. A.1, P_{des} is the design heat load of the building calculated at the outdoor design temperature T_{des}. T_{HLET} is the outdoor air temperature at which the net heat load of the building is equal to zero. For assessing the influence of heat loads on the seasonal performance of heat pumps, the adoption of T_{HLET} = 16 °C is recommended [47]. Following other studies, based on dynamic modeling of a building's thermal loads [48] or through analysis of experimental data [49,50], this value has been estimated to be approximately T_{HLET} = 20 °C. Thus, if the series of outdoor air temperature values at each i^{th} hour during the periods when the heating system is on is known, it is possible to calculate the building's annual heat energy demand through the following summation:

$$E_b = \sum_{i=1}^{N} P_b(i) \quad \text{(A.2)}$$

where N is the total number of plant operating hours in the year.

Nomenclature

Symbols

DHN	District Heating Network
DG	Distributed Generation
HE	Heat Exchanger
m	Flow rate
Q	Heat capacity
UA	Global Heat transfer coefficient

Greek letters

η	Efficiency

Subscripts

h	Hot side of heat exchanger

$_{c}$ Cold side of heat exchanger

$_{n}$ Nominal conditions

$_{ex}$ Referred to experimental test

$_{ext}$ External

$_{sol}$ Referred to the solar collector

Superscripts

* Operation conditions

^{gross} Referred to the gross solar collector surfce

References

[1] Lund H, Østergaard PA, Connolly D, Mathiesen BV. Smart energy and smart energy systems. Energy 2017;137:556–65. https://doi.org/10.1016/J.ENERGY.2017.05.123.

[2] Mendes G, Ioakimidis C, Ferrão P. On the planning and analysis of Integrated Community Energy Systems: A review and survey of available tools. Renew Sustain Energy Rev 2011;15:4836–54. https://doi.org/10.1016/j.rser.2011.07.067.

[3] Revesz A, Jones P, Dunham C, Davies G, Marques C, Matabuena R, et al. Developing novel 5th generation district energy networks. Energy 2020;201:117389. https://doi.org/10.1016/J.ENERGY.2020.117389.

[4] Horstink L, Wittmayer JM, Ng K, Luz GP, Marín-González E, Gährs S, et al. Collective Renewable Energy Prosumers and the Promises of the Energy Union: Taking Stock. Energies 2020, Vol 13, Page 421 2020;13:421. https://doi.org/10.3390/EN13020421.

[5] Jodeiri AM, Goldsworthy MJ, Buffa S, Cozzini M. Role of sustainable heat sources in transition towards fourth generation district heating – A review. Renew Sustain Energy Rev 2022;158:112156. https://doi.org/10.1016/J.RSER.2022.112156.

[6] Brange L, Englund J, Lauenburg P. Prosumers in district heating networks – A Swedish case study. Appl Energy 2016;164:492–500. https://doi.org/10.1016/J.APENERGY.2015.12.020.

[7] Kauko H, Kvalsvik KH, Rohde D, Nord N, Utne Å. Dynamic modeling of local district heating grids with prosumers: A case study for Norway. Energy 2018;151:261–71. https://doi.org/10.1016/J.ENERGY.2018.03.033.

[8] Gross M, Karbasi B, Reiners T, Altieri L, Wagner HJ, Bertsch V. Implementing prosumers into heating networks. Energy 2021;230:120844. https://doi.org/10.1016/J.ENERGY.2021.120844.

[9] Nord N, Shakerin M, Tereshchenko T, Verda V, Borchiellini R. Data informed physical models for district heating grids with distributed heat sources to understand thermal and hydraulic aspects. Energy 2021;222. https://doi.org/10.1016/j.energy.2021.119965.

[10] Brand L, Calvén A, Englund J, Landersjö H, Lauenburg P. Smart district heating networks – A simulation study of prosumers' impact on technical parameters in distribution networks. Appl Energy 2014;129:39–48. https://doi.org/10.1016/J.APENERGY.2014.04.079.

[11] Wang D, Carmeliet J, Orehounig K. Design and Assessment of District Heating Systems with Solar Thermal Prosumers and Thermal Storage. Energies 2021, Vol 14, Page 1184 2021;14:1184. https://doi.org/10.3390/EN14041184.

[12] Huang P, Copertaro B, Zhang X, Shen J, Löfgren I, Rönnelid M, et al. A review of data centers as prosumers in district energy systems: Renewable energy integration and waste heat reuse for district heating. Appl Energy 2020;258. https://doi.org/10.1016/j.apenergy.2019.114109.

[13] Li H, Hou J, Hong T, Nord N. Distinguish between the economic optimal and lowest distribution temperatures for heat-prosumer-based district heating systems with short-term thermal energy storage. Energy 2022;248:123601. https://doi.org/10.1016/J.ENERGY.2022.123601.

[14] Selvakkumaran S, Axelsson L, Svensson IL. Drivers and barriers for prosumer integration in the Swedish district heating sector. Energy Reports 2021;7:193–202. https://doi.org/10.1016/J.EGYR.2021.08.155.

[15] Postnikov I, Stennikov V, Penkovskii A. Prosumer in the district heating systems: Operating and reliability modeling. In: Li H. Chen X. YJYH-X, editor. Energy Procedia, vol. 158, Elsevier Ltd; 2019, p. 2530–5. https://doi.org/10.1016/j.egypro.2019.01.411.

[16] Lickleder T, Hamacher T, Kramer M, Perić VS. Thermohydraulic model of Smart Thermal Grids with bidirectional power flow between prosumers. Energy 2021;230. https://doi.org/10.1016/j.energy.2021.120825.

[17] Gummerus P. New developments in substations for district heating. Adv Dist Heat Cool Syst 2016:215–21. https://doi.org/10.1016/B978-1-78242-374-4.00010-0.

[18] Moallemi A, Arabkoohsar A, Pujatti FJP, Valle RM, Ismail KAR. Non-uniform temperature district heating system with decentralized heat storage units, a reliable solution for heat supply. Energy 2019;167:80–91. https://doi.org/https://doi.org/10.1016/j.energy.2018.10.188.

[19] Yang X, Li H, Svendsen S. Decentralized substations for low-temperature district heating with no Legionella risk, and low return temperatures. Energy 2016;110:65–74.

https://doi.org/https://doi.org/10.1016/j.energy.2015.12.073.

[20] Kim R, Hong Y, Choi Y, Yoon S. System-level fouling detection of district heating substations using virtual-sensor-assisted building automation system. Energy 2021;227:120515. https://doi.org/https://doi.org/10.1016/j.energy.2021.120515.

[21] Ancona MA, Branchini L, Di Pietra B, Melino F, Puglisi G, Zanghirella F. Utilities Substations in Smart District Heating Networks. Energy Procedia 2015;81:597–605. https://doi.org/10.1016/J.EGYPRO.2015.12.044.

[22] Zinsmeister D, Lickleder T, Christange F, Tzscheutschler P, Perić VS. A comparison of prosumer system configurations in district heating networks. Energy Reports 2021;7:430–9. https://doi.org/10.1016/j.egyr.2021.08.085.

[23] Hassine I Ben, Eicker U. Control Aspects of Decentralized Solar Thermal Integration into District Heating Networks. Energy Procedia 2014;48:1055–64. https://doi.org/10.1016/J.EGYPRO.2014.02.120.

[24] Bünning F, Wetter M, Fuchs M, Müller D. Bidirectional low temperature district energy systems with agent-based control: Performance comparison and operation optimization. Appl Energy 2018;209:502–15. https://doi.org/10.1016/J.APENERGY.2017.10.072.

[25] Pipiciello M, Caldera M, Cozzini M, Ancona MA, Melino F, Di Pietra B. Experimental characterization of a prototype of bidirectional substation for district heating with thermal prosumers. Energy 2021;223. https://doi.org/10.1016/j.energy.2021.120036.

[26] Solar Energy Laboratory U of W-M. Trnsys 18. Sol Energy Lab Univ Wisconsin-Madison 2018;3:7–36.

[27] SDH project n.d. https://doi.org/https://www.solar-district-heating.eu/.

[28] SDHp2m project n.d.

[29] Carpaneto E, Lazzeroni P, Repetto M. Optimal integration of solar energy in a district heating network. Renew Energy 2015;75:714–21. https://doi.org/https://doi.org/10.1016/j.renene.2014.10.055.

[30] Palomba V, Dino GE, Frazzica A. Analysis of the Potential of Solar-Assisted Heat Pumps: Technical, Market, and Social Acceptance Aspects. Sol RRL 2022;6:2200037. https://doi.org/https://doi.org/10.1002/solr.202200037.

[31] Palomba V, Dino GE, Frazzica A. Solar-Assisted Heat Pumps and Chillers. Handb. Clim. Chang. Mitig. Adapt., New York, NY: Springer New York; 2021, p. 1–54. https://doi.org/10.1007/978-1-4614-6431-0_116-1.

[32] Cioccolanti L, Renzi M, Comodi G, Rossi M. District heating potential in the case of low-grade waste heat recovery from energy intensive industries. Appl Therm Eng 2021;191:116851.

https://doi.org/https://doi.org/10.1016/j.applthermaleng.2021.116851.

[33] Ancona MA, Branchini L, De Pascale A, Melino F. Smart District Heating: Distributed Generation Systems' Effects on the Network. Energy Procedia 2015;75:1208–13. https://doi.org/10.1016/J.EGYPRO.2015.07.157.

[34] Eric J, Vad B. "Progression of District Heating-1st to 4th generation" n.d.

[35] Winterton RHS. Where did the Dittus and Boelter equation come from? Int J Heat Mass Transf 1998;41:809–10. https://doi.org/10.1016/S0017-9310(97)00177-4.

[36] Schmidt D, Lygnerud K. Low Temperature District Heating as a Key Technology for a Successful Integration of Renewable Heat Sources in our Energy Systems n.d.

[37] Norişor M, Ban D, Pătraşcu R, Minciuc E. COMPLEX, ENERGY, ECONOMIC AND ENVIRONMENTAL ANALYSIS OF DIFFERENT SOLUTIONS FOR INTEGRATING SOLAR THERMAL PANELS (PT) IN TO DISTRICT HEATING SUBSTATION (DHS). UPB Sci Bull, Ser C n.d.;84:2022.

[38] RES DHC project n.d. https://doi.org/https://www.res-dhc.com/it/informazioni/h2020-res-dhc/.

[39] Chèze D, Cuneo A, Macciò C, Porta M, Dino G, Frazzica A, et al. FOUR INNOVATIVE SOLAR COUPLED HEAT PUMP SOLUTIONS FOR BUILDING HEATING AND COOLING 2020. https://doi.org/10.18086/eurosun.2020.04.07.

[40] Database M. Meteonorm Version 8 - Meteonorm (en) n.d. https://meteonorm.com/en/meteonorm-version-8 (accessed March 4, 2021).

[41] Bürger V, Steinbach J, Kranzl L, Müller A. Third party access to district heating systems - Challenges for the practical implementation. Energy Policy 2019;132:881–92. https://doi.org/10.1016/J.ENPOL.2019.06.050.

[42] Pöyry Management Consulting Oy. Third-party access to district heating networks. A report to Finnish Energy 2018:65.

[43] EN 14825:2018 - Air conditioners, liquid chilling packages and heat pumps, with electrically driven n.d. https://standards.iteh.ai/catalog/standards/cen/304fe3bd-b611-4f34-8ca2-8ace2d476d89/en-14825-2018 (accessed January 9, 2023).

[44] UNI/TS 11300-4:2016 - UNI Ente Italiano di Normazione n.d. https://store.uni.com/en/uni-ts-11300-4-2016 (accessed January 9, 2023).

[45] EN 12831:2003 - Heating systems in buildings - Method for calculation of the design heat load n.d. https://standards.iteh.ai/catalog/standards/cen/5a4acdae-ff13-4411-8b0b-b54c65c4f91c/en-12831-2003 (accessed January 9, 2023).

[46] CEN/TR 15615:2008 - Explanation of the general relationship between various European standards and n.d. https://standards.iteh.ai/catalog/standards/cen/d7208116-

9623-4117-8d99-4c81230c6f5e/cen-tr-15615-2008 (accessed January 9, 2023).

[47] Dongellini M, Naldi C, Morini GL. Seasonal performance evaluation of electric air-to-water heat pump systems. Appl Therm Eng 2015;90:1072–81. https://doi.org/https://doi.org/10.1016/j.applthermaleng.2015.03.026.

[48] Grossi I, Dongellini M, Piazzi A, Morini GL. Dynamic modelling and energy performance analysis of an innovative dual-source heat pump system. Appl Therm Eng 2018;142:745–59. https://doi.org/https://doi.org/10.1016/j.applthermaleng.2018.07.022.

[49] Szulgowska-Zgrzywa, Malgorzata, Piechurski, Krzysztof. The influence of thermal load profile of building on the air/water heat pump efficiency simulation. E3S Web Conf 2019;116:89. https://doi.org/10.1051/e3sconf/201911600089.

[50] Cannistraro M, Mainardi E, Bottarelli M. Mathematical Modelling of Engineering Problems Testing a dual-source heat pump 2018;5:205–10.